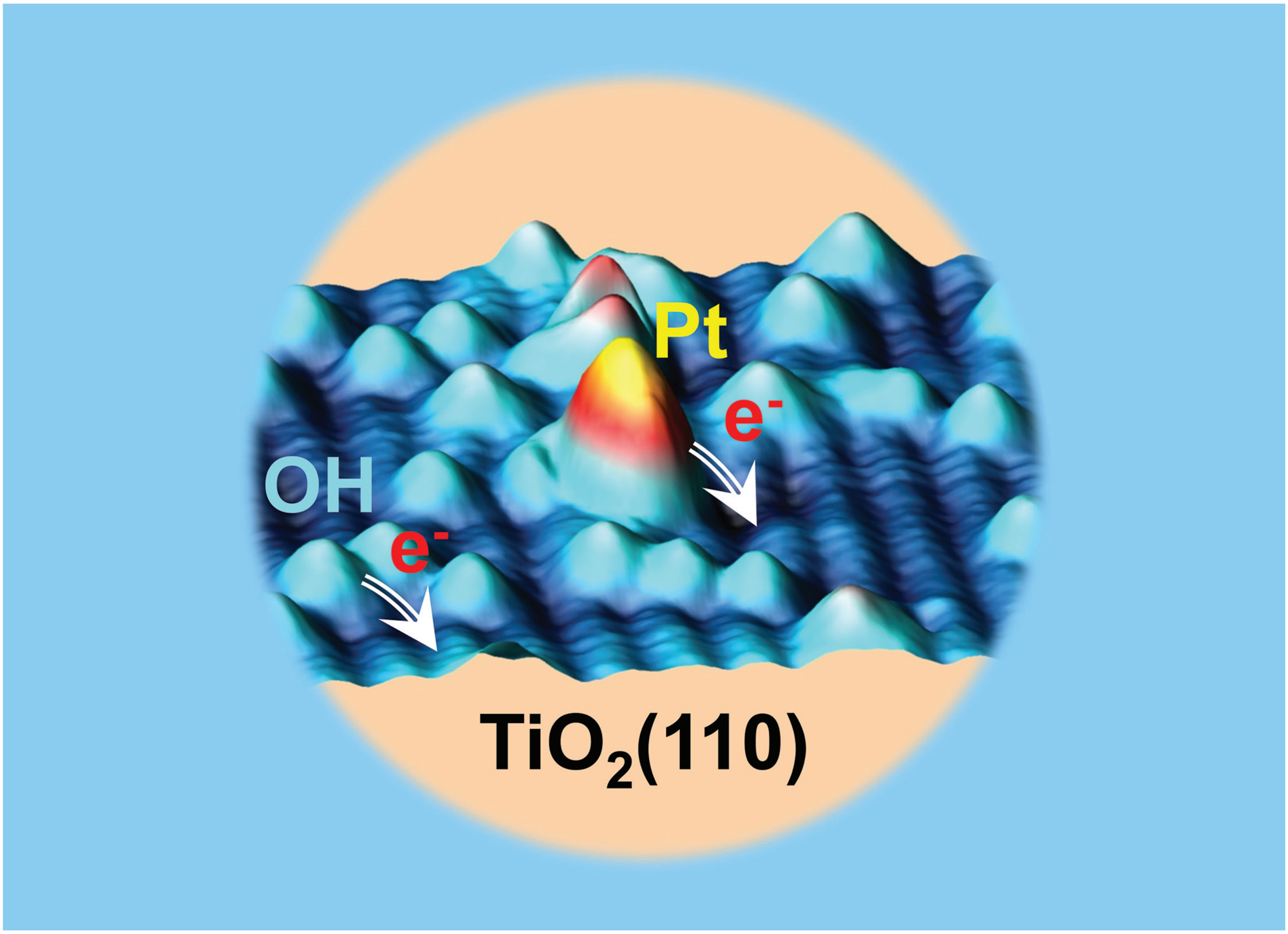

Showcasing research from Osaka University, University of Tokyo, Japan, and Universidad Autónoma de Madrid, Spain.

The local electronic properties of individual Pt atoms adsorbed on TiO_2 (110) studied with Kelvin probe force microscopy and first-principles simulations

We have identified two characteristic regimes in local contact potential difference (LCPD) spectroscopy of Pt atoms on a hydroxylated TiO_2 (110) surface. At far tip-sample distances, LCPD values show a weak distance dependence and can be attributed to the intrinsic charge transfer from Pt to the oxide support. Beyond the onset of short–range chemical interactions, LCPD values exhibit a strong distance dependence that we ascribe to the local structural and charge rearrangements induced by the tip–sample interaction. These findings promote KPFM as a suitable tool for the understanding of electron transfer in catalytically active materials.

As featured in:

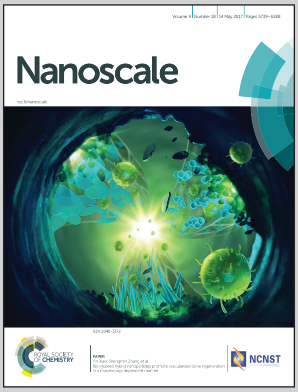

See Ayhan Yurtsever, Rubén Pérez *et al.*, *Nanoscale*, 2017, **9**, 5812.

ROYAL SOCIETY OF CHEMISTRY

rsc.li/nanoscale

Nanoscale

PAPER

View Article Online
View Journal | View Issue

Check for updates

Cite this: *Nanoscale*, 2017, **9**, 5812

The local electronic properties of individual Pt atoms adsorbed on TiO_2(110) studied by Kelvin probe force microscopy and first-principles simulations†

Ayhan Yurtsever,*[a,b,c] Delia Fernández-Torre,[d,e] Jo Onoda,[a,f] Masayuki Abe,[c] Seizo Morita,[a,b] Yoshiaki Sugimoto[a,f] and Rubén Pérez*[d,g]

Noble metal nanostructures dispersed on metal oxide surfaces have applications in diverse areas such as catalysis, chemical sensing, and energy harvesting. Their reactivity, chemical selectivity, stability, and light absorption properties are controlled by the interactions at the metal/oxide interface. Single-atom metal adsorbates on the rutile TiO_2(110)-(1 × 1) surface have become a paradigmatic model to characterize those interactions and to understand the unique electronic properties of these supported nanostructures. We combine Kelvin probe force microscopy (KPFM) experiments and density functional theory (DFT) calculations to investigate the atomic-scale variations in the contact potential difference of individual Pt atoms adsorbed on a hydroxylated (*h*) TiO_2(110)-(1 × 1) surface. Our experiments show a significant drop in the local contact potential difference (LCPD) over Pt atoms with respect to the TiO_2 surface, supporting the presence of an electron transfer from the Pt adsorbates to the substrate. We have identified two characteristic regimes by LCPD spectroscopy. At far tip–sample distances, LCPD values show a weak distance dependence and can be attributed to the intrinsic charge transfer from Pt to the oxide support. Beyond the onset of short-range chemical interactions, LCPD values exhibit a strong distance dependence that we ascribe to the local structural and charge rearrangements induced by the tip–sample interaction. These findings also apply to other electropositive adsorbates such as potassium and the hydrogen atoms forming the OH groups that are present on the *h*-TiO_2(110) surface, promoting KPFM as a suitable tool for the understanding of electron transfer in catalytically active materials.

Received 24th September 2016,
Accepted 9th February 2017

DOI: 10.1039/c6nr07550a

rsc.li/nanoscale

Introduction

Titanium dioxide (TiO_2) surfaces have been extensively used as substrates in a broad range of applications, including heterogeneous catalysis, photocatalysts, surface coating, medical implants, and gas sensors.[1] Noble metal nanostructures with sizes down to single atoms (*e.g.*, platinum and gold) supported on TiO_2 surfaces are of particularly great interest in fundamental as well as in industrial research due to their potential impact in catalysis, photocatalytic hydrogenation, and fuel production.[2–6] The electronic interaction of metal nanoclusters and/or individual atoms with oxide supports and the associated charge transfer and its direction govern many important physical/chemical processes at the metal/oxide interface and determine the chemical reactivity, the selectivity, and the thermal stability of the supported catalysts.[7–11] Surface modification with noble metal nanoclusters has also shown to enhance significantly the sensitivity and selectivity of metal–oxide based gas sensors.[12] Therefore, an atomic-scale understanding of the interactions of metal nanostructures and/or isolated atoms with oxide supports is of central importance

---

[a] *Graduate School of Engineering, Osaka University, 2-1 Yamada Oka, Suita, Osaka 565-0871, Japan. E-mail: ayhan@afm.eei.eng.osaka-u.ac.jp; Fax: +81-6-6850-6662; Tel: +81-6-6850-6304*
[b] *The Institute of Scientific and Industrial Research, Osaka University, 8-1 Mihogaoka, Ibaraki, Osaka 567-0047, Japan*
[c] *Graduate School of Engineering Science, Osaka University, 1-3 Machikaneyama, Toyonaka, Osaka 560-8531, Japan*
[d] *Departamento de Física Teórica de la Materia Condensada, Universidad Autónoma de Madrid, E-28049 Madrid, Spain*
[e] *Instituto de Estructura de la Materia, CSIC, Serrano 121, 28006 Madrid, Spain*
[f] *Department of Advanced Materials Science, Graduate School of Frontier Sciences, University of Tokyo, 5-1-5, Kashiwanoha, Kashiwa, Chiba 277-8561, Japan*
[g] *Condensed Matter Physics Center (IFIMAC), Universidad Autónoma de Madrid, E-28049 Madrid, Spain. E-mail: ruben.perez@uam.es*

† Electronic supplementary information (ESI) available: Additional information related to the additional datasets acquired with different cantilevers and tips; calculated short-range interaction forces above the Pt/TiO_2(110) surface for protrusion- and hole-model tips; constant-height LCPD maps; charge transfer analysis between the model tip and Pt/TiO_2 system; distance dependence of the LCPD above the K atoms adsorbed on the *h*-TiO_2 surface. See DOI: 10.1039/C6NR07550A

for tailoring the electronic properties of metal/oxide nanomaterials in applications for heterogeneous catalysis and chemical sensors.

A good indicator for understanding the nature of the interaction between metals and oxide supports is the work function. The changes in the work function induced by atomic adsorbates are strongly correlated with the adsorbate–substrate charge transfer, and have been traditionally used[13–16] to determine the direction and extent of the global charge exchange at the interface. The key challenge is to extend this insight at the atomic level, determining the modification of the local electronic structure associated with individual adsorbates. Probing the interfacial charge transfer and the work function changes induced by metal adsorbates on TiO_2 can significantly contribute to our understanding of the complex interface properties and chemistry. This information is essential to reveal the fundamental processes behind the enhanced catalytic activity of supported metal nanoclusters, and to design novel nanostructured materials for catalytic applications.

Kelvin probe force microscopy (KPFM) – based on atomic force microscopy (AFM) principles – is the tool of choice to measure the local contact potential difference (LCPD) variations, thereby mapping the work function of the sample with high spatial resolution.[17] Several studies have demonstrated the potential of KPFM to probe local contributions to the contact potential difference on an atomic scale on various surfaces,[18–22] and the theoretical investigations have provided insights into the origin of the atomic-scale LCPD contrast.[22–28] Previously, KPFM has made possible the identification of the charge state of individual adsorbate atoms,[29] molecules,[30] and surface defects.[31] Recently, the range of applications of KPFM was further extended to organic molecules, and the observed LCPD contrast was attributed to differences in the intramolecular charge distribution.[32,33] The presence of subsurface charges on an oxide surface was also realized recently by using KPFM.[34] KPFM has also been employed to explore the charge transfer between deposited metal nanoparticles and their support.[35–38]

Here, we report a study of the atomic-scale lateral and distance variation of the contact potential difference of individual Pt atoms on a hydroxylated rutile $TiO_2(110)$ [h-$TiO_2(110)$] surface. We combine KPFM images with distance-dependent LCPD spectroscopy [$V_{LCPD}(z)$] measurements and first-principles density functional theory (DFT) calculations of the local work function changes as a function of the tip–sample distance for different tip models in order to provide insight into the LCPD contrast in the presence of metal adsorbates and OH groups on this prototypical metal oxide surface. Our results reveal the role played by the tip terminations associated with the different imaging modes (protrusion, hole, and neutral) in the formation of the LCPD contrast and identify two characteristic regimes in the LCPD. At far tip–sample distances, LCPD values, showing a weak distance dependence, can be attributed to the intrinsic charge transfer from Pt to the oxide support. Beyond the onset of short-range chemical interactions, LCPD values exhibit a strong distance dependence that we ascribe to the local structural and charge rearrangements induced by the tip–sample interaction. This interpretation is consistent with our results for other electropositive elements such as potassium adsorbates and the hydrogen atoms adsorbed on the O_{br} atoms, forming OH groups, that are present on the h-TiO_2 surface, and where charge transfer to the substrate has been previously reported. Based on these results, we conclude that the LCPD drop over the Pt sites with reference to the h-TiO_2 substrate supports the presence of a charge transfer from single Pt atoms to the oxide, still a controversial issue in this model system for real catalysts based on metal nanoparticles supported on reducible oxides.

Results and discussion

Non-contact atomic force microscopy (NC-AFM) has been shown to provide a rich variety of atomic contrasts on the rutile h-$TiO_2(110)$ surface,[39–44] which have been referred to as neutral (imaging of bridging oxygen (O_{br}) sites together with hydroxyl (OH) groups as protrusions), hole (imaging of O_{br} rows as bright stripes and OH groups as dark holes), and protrusion modes (imaging of fivefold coordinated Ti (Ti_{5f}) atoms and OH groups as protrusions). Fig. 1(a)–(f) show the typical NC-AFM topography and the corresponding KPFM images of the h-$TiO_2(110)$ surfaces, displaying the most frequently observed atomic contrasts. KPFM images, taken with an active Kelvin feedback (see Methods), provide (x,y) maps of the LCPD between the tip and the sample at a certain frequency shift (Δf) set point. Fig. 1(a) and (b) were recorded with a tip providing protrusion mode contrast. The corresponding KPFM image

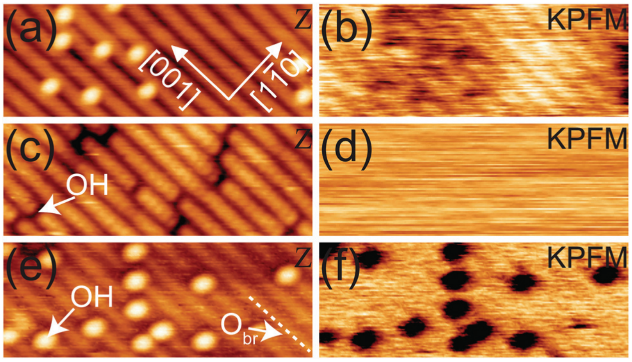

Fig. 1 NC-AFM topographic (Z) and simultaneously measured KPFM images of the h-$TiO_2(110)$ surface at room temperature, acquired with three tips with different atomic terminations: (a, b) for protrusion mode, (c, d) for hole mode, and (e, f) for neutral mode tips. The bright/dark features on the bridging oxygen (O_{br}) rows are due to surface OH groups. The contrast above OH sites in the LCPD map in (b) and (f) is shifted to lower LCPD values compared to the substrate, while in (d) no discriminable LCPD contrast is observed above OH sites. The acquisition parameters were as follows: (a, b) f_0 = 163.662 kHz and A = 16.7 nm; (c, d) f_0 = 163.662 kHz and A = 16.7 nm; (e, f) f_0 = 155.531 kHz and A = 13.0 nm. Image parameters: (a, b) 9.8 × 3.6 nm^2 and Δf = −2.5 Hz; (c, d) 9.8 × 3.6 nm^2 and Δf = −1.2 Hz; (e, f) 9.8 × 3.6 nm^2 and Δf = −1.2 Hz. KPFM parameters: U_{ac} = 0.2–0.5 V, f_{ac} = 500 Hz.

in Fig. 1(b) exhibits a clear distinction of the LCPD contrast between the surface atomic rows, reflecting the variation of the local charge distribution of the alternating O_{br} and Ti_{5f} atomic rows along the [001] surface crystallographic direction. It should be noted here that the presence of the OH groups on the surface enables the unambiguous identification of the surface ionic sublattice in the LCPD map. The LCPD map recorded by a protrusion mode tip is not in phase with the surface topograph, and reflects the O_{br} atomic rows as bright stripes (higher LCPD) and the Ti_{5f} as dark stripes (lower LCPD). This is in good agreement with the result reported in ref. 18, although in that study, individual OH impurity defects were not resolved.

Most importantly, the atomic hydrogens in the OH groups are also clearly resolved in the LCPD map. The individual hydrogen atoms reduce locally the LCPD over O_{br} by about 10 to 20 mV, which tentatively points to a positive charge on H atoms. This charge transfer is consistent with recent valence band photoemission measurements reporting an increase of the band gap shift in the surface spectra by the adsorption of H adatoms on O_{br}.[45] This increase can be understood in terms of a charge transfer from the H adatoms to the surface that leaves the H atoms as positively charged adsorbates. We have repeated these measurements with other tips that display protrusion mode contrast. In all the cases, the KPFM images show the same basic features, with a clear distinction of the O_{br} and Ti_{5f} surface atomic rows, and a local reduction of the LCPD on the OH sites with respect to the substrate (see ESI Fig. S1†).

For reliable KPFM measurements, it is very important to explore the influence of the distinct tip states on the measured LCPD contrast. Therefore, we have used other tip–apex terminations that generate the neutral and hole mode imaging contrast of the surface to register an image of the LCPD map above the *h*-TiO_2(110) surface. We have obtained a similar tendency of the LCPD shift with a neutral mode tip (see Fig. 1(f) and S2†), displaying a higher LCPD over O_{br} and a lower LCPD over OH groups with a more pronounced contrast (~350 mV). On the other hand, the LCPD map provided by a hole imaging mode tip does not show a discernible potential signal over OH sites or the surface atomic rows, even at different imaging set points (see Fig. 1(c) and (d)).

As a next step, we investigate the LCPD variation induced by the adsorption of individual Pt atoms on the *h*-TiO_2(110) surface. A typical NC-AFM topography image of the individual Pt atoms at room temperature (RT), obtained after exposure of the *h*-TiO_2(110) surface to Pt, is shown in Fig. 2(a). The Pt atoms, which appear as bright elongated features, preferentially adsorb at the center of the Ti_{5f} rows and are confined between two O_{br} rows.[46] This is in good agreement with the results of previous theoretical studies[47–49] and also with the observations by aberration-corrected scanning transmission electron microscopy imaging.[50] The elongated appearance of the Pt atoms in the NC-AFM images has been explained by the diffusion of Pt atoms in a very local region along one-dimensional channels connecting the two favorable atomic sites on the *h*-TiO_2(110) surface.[46,48] The corresponding KPFM image in Fig. 2(b) exhibits an atomic contrast with a lower LCPD above the Pt atom site with respect to the surrounding TiO_2 substrate. For a comparison, we have also investigated the LCPD variation over the potassium (K) atoms with an identical tip termination providing the protrusion mode image (Fig. 2(c)). It has been well-established from the spectroscopic measurements that the adsorption process is accompanied by a complete charge transfer from K to the substrate at low K coverage,[51] with K becoming a positively charged ion. This has also been confirmed by the photoemission spectra,[52] which show the K-induced band-gap states at 0.9 ± 0.1 eV. The occurrence of such charge transfer was evidenced by our KPFM measurements on the K/TiO_2 surface (see Fig. 2(d)), which indicate a reduction in the LCPD at the K atoms with respect to the supporting TiO_2 surface, as for the Pt atoms. According to the classical Langmuir model,[53] the lowering of the LCPD implies the presence of surface dipoles with a component

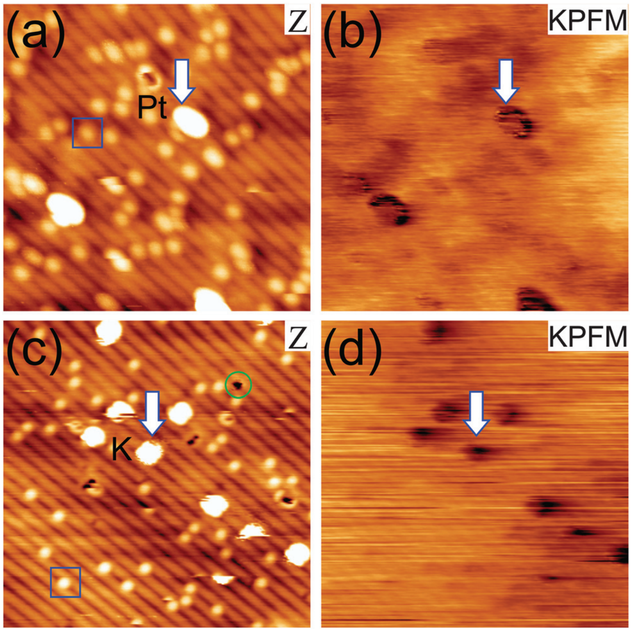

Fig. 2 NC-AFM topography (*Z*) and simultaneously measured KPFM images of the *h*-TiO_2(110) surface exposed to a low-coverage of (a, b) Pt and (c, d) K atoms, recorded with a tip generating protrusion mode image contrast. A clear depression over Pt and K atomic positions appears in the LCPD map, indicating that the Kelvin potential over these sites is more negative compared to the supporting TiO_2 substrate. We note that the LCPD map over the Pt atom position in (b) appears as a ring-like structure. We attribute this to a tip-induced effect (see the ESI,† for further discussion). The white arrows indicate single Pt and K atoms. The blue square in (a) and (c) indicates the surface OH groups. A small number of dark features also appear in (c), one of which is highlighted with a green circle. We attribute this to an image artifact caused by contrast inversion as the tip enters the repulsive region of the short-range interaction forces when probing a protruding atomic species. The acquisition parameters were as follows: (a, b) f_0 = 166.426 kHz and A = 6.45 nm; (c, d) f_0 = 163.662 kHz and A = 16.7 nm. Image parameters: (a, b) 15 × 15 nm^2 and $\Delta f = -14.4$ Hz; (c, d) 15 × 15 nm^2 and $\Delta f = -2.5$ Hz. KPFM parameters: U_{ac} = 0.2–0.5 V, f_{ac} = 500 Hz.

pointing outward, which in turn indicates that the Pt and K atoms behave as positively charged adsorbates. This is also in line with the concept of the KPFM working principle, the sample has to be biased more negatively to compensate positive charges on the Pt and K atoms. The LCPD features described above are well reproduced with other tips providing protrusion mode contrast. On the contrary, the KPFM images (not shown here) generated by a hole mode tip do not indicate any visible changes associated with the LCPD over Pt as well as on K atom sites with respect to the supporting TiO_2 surface, similarly to what we have observed for the OH groups on the pristine TiO_2 surface (Fig. 1(d)).

There is a long-standing debate over the interpretation of the atomic-scale contrast in KPFM images, and, in particular, the role of the tip,[21,22,54] the influence of interactions different from the purely electrostatic ones,[23,55,56] and the presence of (instrumental) potential artifacts.[57] Distance-dependent KPFM measurements on semiconductors[20] and molecules[33] have provided significant insight. This is the route that we have followed in our oxide system. We have performed force and distance-dependent LCPD spectroscopy [V_{LCPD} (z)] measurements with two distinct types of tips (protrusion and hole) that provide different contrast for the topography and KPFM images. It needs to be noted that the neutral mode tips were not stable enough for spectroscopy measurements. We had difficulties in performing force spectroscopy measurements with neutral mode tips due to tip changes during the force curve acquisition, implying that these tips have a strong tendency to contamination with surface materials. Therefore, it is extremely difficult to collect reliable force and LCPD spectroscopy data with neutral mode tips. Fig. 3(a) and (b) show the simultaneously measured short-range force (F_{SR} (z)) and V_{LCPD} (z) curves obtained using an active Kelvin feedback (see Methods) at single Pt, O_{br}, Ti_{5f}, and OH surface defect sites acquired with a tip generating the protrusion mode image. The z-axis of both F_{SR} (z) and V_{LCPD} (z) curves has been shifted to take into account the topographic correction over the Pt atom, setting a common origin for all the sites. The final distance reference has been determined by aligning the attractive force maxima on the Pt atom with the theoretically calculated results (see ESI Fig. S3(c)†), as discussed in ref. 46. The LCPD signals over both Pt atoms and OH groups reveal a reduction from the mean Kelvin signal of the surrounding TiO_2 substrate as the tip approaches the sample.

The V_{LCPD} (z) curves in Fig. 3(b) clearly display two different regimes. For distances larger than 5.2 Å the curve over Pt shows a weak distance dependence, with a variation of only ~0.1 V from the LCPD at 6.2 Å, while the LCPD over the OH site remains essentially constant within this distance range. Below 5.2 Å there is a sharp drop in the Pt LCPD curve (see the arrow in Fig. 3(b)), followed by a rapid decrease in distance (0.5 V in ~0.9 Å), reaching a minimum around 4.3 Å, and increasing rapidly for shorter distances. The OH LCPD curve shows a similar trend, with a smaller decrease to a minimum at ~3 Å, and increasing again when we further approach the substrate. At variance, LCPD curves on the O_{br} and Ti_{5f} sites

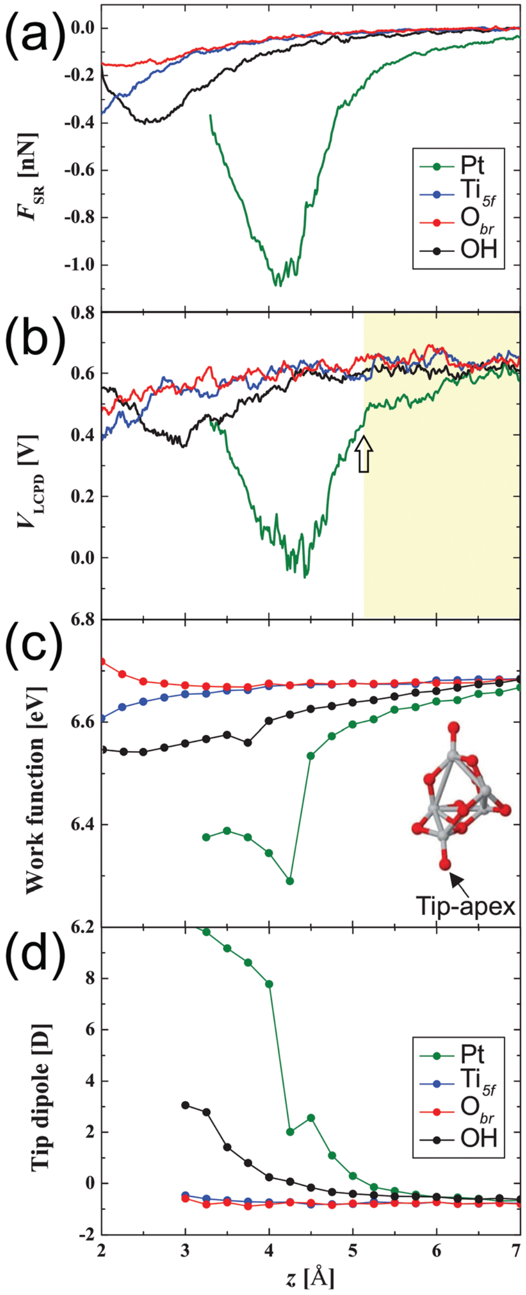

Fig. 3 (a) Experimental short-range forces over Pt (green line), hydroxyl (OH) (black line), O_{br} (red line), and Ti_{5f} (blue line) sites acquired with a protrusion mode tip. (b) Distance-dependent variation of the LCPD acquired over the same atomic positions considered in (a) using an active KPFM feedback to nullify the existing electrostatic forces at each particular distance. Calculated (c) variation of the local work function and (d) change of tip dipole moment upon approaching the protrusion-model tip over the Pt, OH, O_{br}, and Ti_{5f} sites. The region highlighted by a yellow transparent color indicates the intrinsic LCPD due to Pt atom charge transfer. Inset: The ball-and-stick model of the tip structure used in simulation, showing the O-terminated TiO_2-based cluster tip. The z-axis of curves in (a) and (b) has been shifted to take into account the topographic correction over the Pt atom. The final distance reference has been determined by aligning the attractive force maxima on the Pt atom with the theoretically calculated results. Acquisition parameters: f_0 = 160.171 kHz, A = 12.3 nm, Δf = −3.36 Hz. KPFM parameters: U_{ac} = 0.5 V, f_{ac} = 500 Hz.

remain almost constant across the whole distance range explored in the experiments. The comparison with the F_{SR} (z) curves in Fig. 3(a) shows that the abrupt LCPD drop over Pt and the subsequent strong variation occur at distances where the short-range chemical force starts to increase rapidly. Both force and LCPD curves reach extreme values at roughly the same distance, and follow the same distance dependence as we approach the substrate. The same correlation is found for the OH site, with both curves showing the same characteristic distance dependence. The reproducibility of the characteristic LCPD variation on the Pt and OH sites was investigated with different cantilevers and tips providing protrusion mode contrast (see an example in Fig. S3(b)†). The main findings are well reproduced in different experimental runs: the presence of two different regimes, the correlation of the LCPD distance variation with the short-range forces, and the significantly smaller LCPD values associated with Pt atoms compared to the OH and surface sites. While the LCPD variation in the far distance regime seems to be very similar in all the cases, the shape of the curve and the minimum LCPD value are rather dependent on the particular tip used. We have also investigated the V_{LCPD} (z) variation on K atoms deposited on the *h*-TiO_2 surface with a similar tip termination (see topography and KPFM images with a protrusion mode (Fig. S6†) and a neutral mode (Fig. S7†) tip). The LCPD *vs.* distance results display an identical behavior to that found on the Pt atom (see Fig. S8†), with the rapidly varying regime starting around 4 Å. The shape of the V_{LCPD} (z) curves on K and OH sites very much resembles those in Fig. 3(b) and S3(b),† thus corroborating the generality of our results. From the distance analysis presented above, we conclude that the LCPD contrast measured in our KPFM experiments with protrusion mode tips in the far distance regime can be attributed to the local changes in the surface potential due to the intrinsic charge transfer between the adatoms and the substrate. This result is consistent with the tip-independent nature of the LCPD contrast reported on an ionic crystal surface.[22] The direction of the LCPD shift on the OH and Pt atom sites, also identical to that on the K atom, is consistent with the assumption that both Pt and K adsorbates and the OH group are positively charged and, therefore, tend to reduce the surface local work function. As discussed below, we think that the evolution (further reduction) of the LCPD signal at closer distances is related to charge rearrangements induced by the enhanced tip–sample interaction that are very sensitive to both the nature of the tip and the approached atom.

Our KPFM measurements shed light on the nature of the charge transfer between a single Pt atom and a hydroxylated TiO_2 surface that is still a controversial issue. Charge transfer from a Pt atom to a Ti^{4+} ion at the metal/TiO_2 interface has been proposed in ref. 58 based on electron magnetic resonance spectra, while other studies have reported charge transfer from the support to the metal Pt.[59,60] A later study correlated the charge exchange with the surface condition: no significant charge transfer was detected for Pt on a stoichiometric TiO_2 sample, whereas a complete electron transfer from Ti^{3+} to a Pt atom was reported for a reduced sample.[61] On the other hand, a combined NC-AFM and KPFM study[62] concluded that Pt atoms at the O_{br} vacancy site donate charges to the substrate, which is inconsistent with the previous experimental results[59–61] and the recent theoretical studies.[63,64] This discrepancy could be due to the fact that the bright features interpreted as Pt in ref. 62 are, in fact, mostly H atoms in the OH groups. Latter investigations[47,48,64,65] and our own theoretical calculations clearly exclude the adsorption of Pt atoms on top of the O_{br} site. Pt atoms prefer to adsorb at a hollow site between two in-plane oxygen (O_{in}) atoms with the Pt atom bound to one Ti_{5f} and one O_{br} atom on the TiO_2 surface. Another site, on top of an O_{in} atom where the Pt atom is bonded simultaneously to an O_{in} and to a Ti_{5f} atom, has also been reported. These results are confirmed by our experiments, where Pt atoms are found to be located on the Ti_{5f} atomic rows and are confined between two O_{br} atomic rows. Furthermore, single Pt atoms can be clearly distinguished from H adsorbates due to their characteristic appearance in NC-AFM images obtained with tips with different apex structures (leading to three qualitatively different contrast modes), as we have done in our previous work.[46] Based on this evidence, we can conclude that the bright features appearing on the O_{br} atomic rows in Fig. 4(a) of ref. 62 are unarguably H atoms in the OH groups, rather than Pt atoms, imaged by a tip generating protrusion mode contrast of the TiO_2 surface. We want to stress here the importance of recording images of the same surface area with different contrast modes. Using these images we can clearly differentiate between Pt atoms and OH groups as shown by our work.

The significant drop in the LCPD on a single Pt atom found in both our KPFM images and the V_{LCPD} curves clearly supports the charge transfer from the Pt atoms to the oxide surface. This result agrees with the recent case studies of Pt clusters on the $TiO_2(110)$ surface.[66,67] This charge exchange is also consistent with theoretical studies[46,48,63] where the adsorption of a single Pt atom on the $TiO_2(110)$ surface is accompanied by some degree of charge transfer from the Pt atom to the surface. This charge transfer creates a local dipole moment, pointing away from the surface to the vacuum, that is responsible for the direction of the LCPD shift in both the KPFM image (Fig. 2(b)) and the slowly varying regime of the V_{LCPD} (z) curve (the 6–5.2 Å distance range highlighted in Fig. 3(b)).

A completely different behavior is observed when performing the LCPD measurements with a hole mode tip. Fig. 4(a) and (b) show the F_{SR} (z) and V_{LCPD} (z) curves measured above the Pt and O_{br} atoms. The LCPD does not change and gives identical values for both atoms over a distance range between 7 and 3.5 Å. It is only beyond the maximum of the Pt F_{SR} that an increment in the LCPD on the Pt atom is observed. As the tip further approaches the surface, a clear distinction in the LCPD values between the Pt atom and the surface O_{br} rows can be attained. However, imaging at such close distances would generate a strong enhancement of the lateral interaction force that would result in unwanted modifications in either the tip

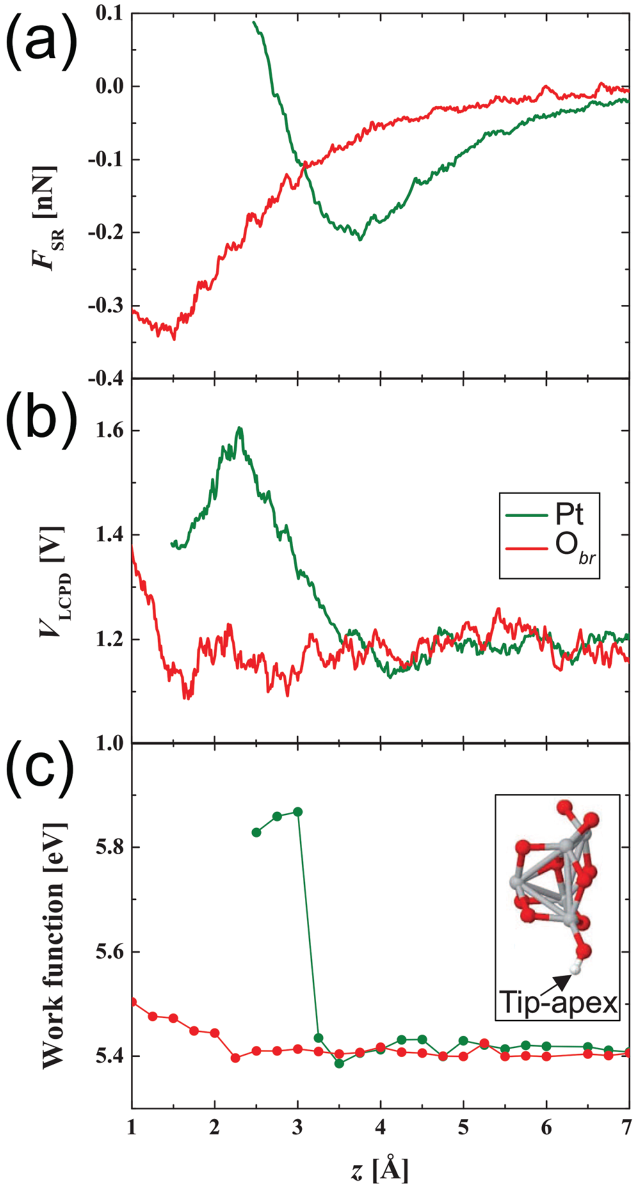

Fig. 4 (a) Experimental short-range interaction forces over Pt (green line) and O_{br} (red line) sites acquired with a tip generating hole mode imaging contrast. (b) Distance dependence of the LCPD above the Pt and O_{br} atoms acquired simultaneously with force spectroscopy data shown in (a). (c) Calculated variation of the local work function upon approaching the hole-model tip over the Pt and O_{br} atoms. Inset shows the ball-and-stick model of the tip structure used in first-principles calculations, showing the OH-terminated TiO_2-based cluster tip. The tip–sample distance in the experimental curves has been shifted to align the attractive force maxima of the Pt atom with the theoretical calculations. Acquisition parameters: f_0 = 158.335 kHz, A = 16.9 nm, Δf = −3.36 Hz. KPFM parameters: U_{ac} = 0.5 V, f_{ac} = 500 Hz.

or surface structures during the scan. Furthermore, the NC-AFM feedback would have problems working at such close distances where the slope of Δf might be inverted in some positions. Thus, KPFM image acquisition is limited to distances close to the onset of the short-range interaction force, where LCPD has identical values on the Pt and O_{br} atoms, explaining the absence of atomic-scale contrast in the KPFM images.

In order to unravel the underlying mechanism of the atomic-scale contrast in the LCPD and the role of tips on the distance dependence of the LCPD signal, we have performed DFT calculations using the VASP code[68] (see Methods for the technical details). Our theoretical approach is based on the link between the LCPD and the work function changes. We determine the variation of the local work function in the presence of the tip using its definition as the energy difference between the Coulomb potential in a vacuum and the Fermi level of the combined tip and surface system that we extract from our DFT calculations for each tip position. Changes in the local work function should reflect the lateral and distance variation of the LCPD obtained in the experiments. It has to be noticed that a proper theoretical treatment of KPFM, as the one described in ref. 27 is extremely challenging as it should include the effects associated with the macroscopic electric field created by the applied bias. These effects result in a long-range contribution to the force (that is essentially site-independent), and, more importantly, a contribution to the short-range force due to the extra polarization added by the macroscopic electric field. Our approach disregards this last term as the response to the electrostatic field created by the tip apex is expected to be dominant. As discussed below, our theoretical results do capture the main trends in the magnitude and distance evolution of the LCPD but are systematically smaller than those found in the experiments, particularly for the most polarizable Pt site. It is likely that the inclusion of the macroscopic electric field and the associated polarization would bring a better quantitative agreement between theory and experiment.

The tips used to evaluate the work function changes are small $(TiO_2)_5$ clusters oriented to expose a singly coordinated O (for protrusion mode) or an OH group (for hole mode) pointing towards the surface. We have shown that these tips reproduce the topography images and force spectroscopy results for the protrusion and hole mode contrast.[43] Besides TiO_2-based clusters, we also considered tips modeled by silicon-based clusters with their apices contaminated with singly and/or doubly bonded O or H atoms or an OH functional group. While the contaminated Si tips can, in principle, be compatible with the forces and associated contrast modes at typical imaging distances, they failed to reproduce the force data close to the force minima in the case of protrusion and hole imaging modes on the *h*-TiO_2(110) surface. These theoretical results do not contradict the fact that sputtered Si tips are initially used in the experiment. Imaging oxides with atomic resolution requires working at close distance to the surface. Under these conditions, accidental contact with the surface and tip contamination are very likely as confirmed by the frequent contrast changes in the experiments.

Our DFT results for the local work function changes (see Fig. 3(c) and 4(c)) reproduce well the trends in the LCPD changes found in our experiments for the full distance range and for both tip models. For the protrusion mode (Fig. 3(c)), the shape of the local work function variation as a function of distance nicely follows the LCPD variation extracted from the experiments, with work function values at the Pt adatom position lower than those on the OH and substrate. On the other hand, the work function change obtained with a hole mode tip (*i.e.*, OH terminated TiO_2 cluster tip) (Fig. 4(c)) also reproduces the experimental results: it displays the same constant value for both the Pt and O_{br} sites up to 3.5 Å, where it starts raising on the Pt site when the tip enters the repulsive branch of the interaction force (see Fig. S4 of the ESI† for the calculated forces).

The work function change induced by an adsorbate is determined by the surface dipole which results from the local charge redistribution at the interface.[53] In order to understand our results and to find a possible correlation between the change in LCPD observed in the experiments and the local electronic structure modifications induced by the interaction of the tip with the Pt/*h*-TiO_2(110) surface, we have investigated the evolution of the tip and/or surface dipole moment directed along the surface normal while approaching the model tips toward the surface. Fig. 3(d) displays the resulting tip local dipole moment change induced upon approaching the protrusion-model tip over the Pt, OH, O_{br}, and Ti_{5f} sites. The tip dipole moment remains essentially constant in the distance range from 7 to 3 Å when the tip approaches over O_{br} and Ti_{5f} atomic rows, while there is an steady increment in the tip dipole moment over the Pt and OH sites for tip–sample distances shorter than 5.5 Å. As can be seen in Fig. 3(c) and (d), the distance range where changes in the local work function take place matches well with the interaction distances associated with the changes in the tip/surface dipole moment. Since these two quantities, *i.e.*, work function and tip dipole change, are obtained in an independent way, the results in Fig. 3(c) and (d) clearly unveil a strong correlation between an increase in the tip local dipole moment and a decrease of the local work function during the approach of the tip to Pt and OH atomic sites.

The difference in the LCPD behavior between the protrusion and hole mode tip is associated with a quite different response of the charge density distribution to the tip–sample interaction. The hole mode tip is rather inert compared to the protrusion mode tip, as shown by the significantly smaller short-range forces (see Fig. 4(a) and S4†), and no significant changes in the tip dipole are found for distances larger than 3.5 Å. This is consistent with the constant value for the local work function found for both the Pt and O_{br} sites in our calculations and in the experiments. This points out the significant role of the tip polarizability in the contrast observed at closer distances.[24]

Our calculations for the protrusion mode tip further reveal a significant charge transfer from the tip to the surface at the onset of short-range interaction at the position of Pt and OH sites (see Fig. S5†). At distances around $z \sim 4.0$–5.5 Å, a charge accumulation between Pt and the closest tip atom is observed, which is indicative of the collapse of the vacuum barrier and the onset of a chemical bond between the O atom at the tip apex and Pt (see the inset of Fig. 3(c) and S3(c)†). The formation of such a chemical bonding state between the tip and surface facilitates the charge density polarization across the interface.[20] This results in a drastic change in the local dipole moment of the tip and adsorbate/surface conjugate system, which, in turn, leads to further modifications in the local work function and to the LCPD variation. Based on these results, together with the distance-dependent LCPD shift, we conclude that the LCPD variation along the tip–sample distance shows two different regimes: (i) for distances above the onset of strong short-range interactions, there is an intrinsic LCPD due to Pt atom charge transfer, (ii) for shorter distances, the LCPD is significantly influenced by the local change of the electronic structure induced by the interaction between the tip and Pt/TiO_2 system. Our results provide support for the theoretical semi-empirical approach developed in ref. 55, where the authors introduce an additional chemical force, associated with the orbital hybridization taking place at short distances, to the multipole electrostatic interaction, in order to reproduce the atomic-scale resolution in KPFM images on semiconductor surfaces.

Conclusions

In conclusion, we have measured the spatial variation of the LCPD of individual Pt atoms on *h*-TiO_2 surfaces. The atomic-scale LCPD maps provided by different tip terminations, associated with distinct topographic contrasts, show the same qualitative behavior. However, the magnitude of the LCPD shift shows a strong tip dependence, and, in the case of tips producing hole mode contrast, seems to completely disappear. A closer inspection of the V_{LCPD} spectroscopic curves has revealed two characteristic regimes with distinctly different distance dependence. At far tip–sample distances, LCPD values, showing the weak distance dependence, were attributed to the intrinsic charge transfer from Pt to the oxide support. Beyond the onset of short-range chemical interactions, LCPD values exhibit a strong distance dependence that we ascribed to the local structural and charge rearrangements induced by the tip–sample interaction. This interpretation is supported by our DFT calculations of the changes in the local work function as a function of tip–sample distance for two tip models that reproduce the image contrast and force spectroscopy measured in the protrusion and hole imaging modes. Our DFT calculations reproduce remarkably well the important qualitative trends in the LCPD distance variation found in our experiments. We have identified a strong correlation between the variation of the tip local dipole moment directed along the surface normal and the local work function change as the tip approaches the sample surfaces. The electronic modification induced by the tip–sample interaction in close proximity reinforces the effect of the intrinsic dipole resulting from the Pt atom charge transfer to the TiO_2 substrate, and reduces further the local work function on the Pt atom.

Our combined experimental and theoretical analysis shows that, although affected by the details of the tip structure at closer distances, KPFM measurements of the local work function variation induced by atomic adsorbates at typical imaging distances can be ascribed to the intrinsic adsorbate/substrate charge transfer. In particular, the lower LCPD measured over the Pt atom compared to the *h*-TiO_2 substrate supports that the Pt atoms are positively charged by electron transfer from the Pt to the substrate. These results shed new light on our understanding of work function changes induced by atomic adsorbates, underline the importance of the appropriate choice of AFM tips for obtaining atomic-scale resolution on the LCPD maps on oxide surfaces, and promote KPFM as a suitable tool for the characterization and fundamental understanding of electron transfer in supported catalysts and organic solar cells where oxide substrates play a key role.

Methods

Experimental details

We performed our experiments in an ultrahigh-vacuum (UHV) chamber (with a base pressure of at least 5×10^{-11} Torr), equipped with a custom built NC-AFM operated at RT. The NC-AFM was operated using the frequency modulation detection mode,[69] keeping the cantilever oscillation amplitude constant. For topographic imaging and KPFM measurements, we used conductive silicon cantilevers, which were cleaned *via* Ar-ion sputtering to remove the native oxide layer and other contaminants. The clean rutile $TiO_2(110)$ crystal (purchased from Shinkosha) was prepared using repeated cycles of Ar^+ ion bombardment (2 keV, 3×10^{-6} Torr) for approximately 5 min at RT and annealed to approximately 1100 K for 1 min to restore a flat substrate surface. When the substrate was cooled down to RT after the final annealing process, Pt atoms were evaporated onto the TiO_2 surface by resistively heating a Ta wire coiled up with high purity Pt (99.995%). Prior to deposition, the Pt source was thoroughly outgassed in UHV at high temperatures, and the typical Pt deposition condition was adjusted to a heating current of ~7.6–7.9 A and an adsorption time of at least ~2 min, with the pressure kept at $\lesssim 3 \times 10^{-10}$ Torr during the deposition. The K atoms were deposited onto the substrate by heating a SAES Getter source (previously outgassed) located approximately 10 cm apart from the sample, with the pressure kept at $\lesssim 2 \times 10^{-10}$ Torr during the deposition.

The KPFM measurements were conducted in the frequency modulation mode (FM-KPFM) in which a dc (U_{dc}) and an ac voltage (U_{ac}) with frequency (f_{ac}) were applied to the sample with the tip being grounded. Our approach, different from other ref. 22, 32 and 33 uses active Kelvin feedback in Kelvin imaging as well as spectroscopic measurements. In the KPFM images, the applied bias voltage is varied in order to determine the compensating voltage dynamically at each scanning point by using an additional feedback operation (Kelvin compensation). Since the compensation bias voltage was applied to the sample, the observed LCPD contrast has the same contrast as the local work function. Site-specific force spectroscopy measurements with KPFM compensation were carried out by recording the Δf with respect to the f_0 as a function of tip–sample relative distance (z). The details of force conversion and the method for the extraction of a long-range force from the total forces can be found in ref. 43. The detailed setup for KPFM as well as distance-dependent bias spectroscopy measurements is described in ref. 20 and 70.

Computational details

Our calculations are based on density functional theory (DFT) as implemented in the VASP 5.2.12 code.[68] Our previous work[43] showed that the Perdew–Burke–Ernzernhof (PBE)[71] functional combined with the projector-augmented-wave (PAW) method and a plane-wave cut-off of 400 eV gives satisfactory results for the simulation of NC-AFM experiments on the $TiO_2(110)$-(1×1) surface, also including the case where a Pt adsorbate is present.[46] Here we maintain the same approach and use the same calculation parameters for energy and force convergence and *k*-sampling. To represent the protrusion and hole mode imaging tips, we rely on the structural models used in our previous studies to explain the force spectroscopy curves associated with the protrusion and hole modes over a broad range of tip–sample distances.[43,46] The models consist of small TiO_2 clusters terminated with an oxygen atom and a hydroxyl group, respectively. We vary the tip–sample distance by focusing the tip onto the surface in a quasi-static way, in steps of 0.25 Å, letting the lowermost tip atoms and uppermost slab atoms free to relax for each step until the forces are smaller than 0.02 eV $Å^{-1}$. To calculate the tip/surface dipole along the surface normal for the various distances, we evaluate the Bader charges for each atom and calculate the corresponding dipole moment using the atomic positions and the corresponding charges. Finally, the work-function is calculated by subtracting the Fermi energy from the vacuum level for each tip–sample model system and every tip–sample distance. We estimate the Fermi level as the energy of the last occupied state and the vacuum level as the average electrostatic potential on a plane parallel to the surface and located in the center of the vacuum region.

Acknowledgements

This work was supported by a Grant-in-Aid for JSPS Fellows (14J00689) and for Scientific Research (25106002, 16H03872, 16K13615, 16H00959, 16H00933, 15H03566, 16K13680, and 16K17482) from the Ministry of Education, Culture, Sports, Science and Technology of Japan (MEXT), the Funding Program for Next Generation World-Leading Researchers, and the Spanish MINECO (projects PLE2009-0061, CSD2010-00024 and MAT2014-54484-P). Computer time was provided by the Spanish Supercomputer Network (RES) at the Marenostrum III (BSC, Barcelona), Magerit (CesViMa, Madrid) and Altamira (SSC, Santander) computers.

References

1 U. Diebold, *Surf. Sci. Rep.*, 2003, **48**, 53–229.

2 M. S. Chen and D. W. Goodman, *Science*, 2004, **306**, 252–255.

3 M. Valden, X. Lai and D. W. Goodman, *Science*, 1998, **281**, 1647–1650.

4 A. Bruix, Y. Lykhach, I. Matolínová, A. Neitzel, T. Skála, N. Tsud, M. Vorokhta, V. Stetsovych, K. Ševčíková, J. Mysliveček, R. Fiala, M. Václavů, K. C. Prince, S. Bruyére, V. Potin, F. Illas, V. Matolín, J. Libuda and K. M. Neyman, *Angew. Chem., Int. Ed.*, 2014, **53**, 10525–10530.

5 H. Sakurai, A. Ueda, T. Kobayashi and M. Haruta, *Chem. Commun.*, 1997, 271–272.

6 M. Anpo and M. Takeuchi, *J. Catal.* 2003, **216**, 505–516.

7 G. Pacchioni, *Phys. Chem. Chem. Phys.*, 2013, **15**, 1737–1757.

8 A. Bruix, J. A. Rodriguez, P. J. Ramírez, S. D. Senanayake, J. Evans, J. B. Park, D. Stacchiola, P. Liu, J. Hrbek and F. Illas, *J. Am. Chem. Soc.*, 2012, **134**, 8968–8974.

9 O. Dulub, W. Hebenstreit and U. Diebold, *Phys. Rev. Lett.*, 2000, **84**, 3646–3649.

10 A. L. Linsebigler, G. Lu and J. T. Yates, *Chem. Rev.*, 1995, **95**, 735–758.

11 A. T. Bell, *Science*, 2003, **299**, 1688–1691.

12 A. Kolmakov, D. O. Klenov, Y. Lilach, S. Stemmer and M. Moskovits, *Nano Lett.*, 2005, **5**, 667–673.

13 A. Michaelides, P. Hu, M.-H. Lee, A. Alavi and D. A. King, *Phys. Rev. Lett.*, 2003, **90**, 246103.

14 T. Roman and A. Groß, *Phys. Rev. Lett.*, 2013, **110**, 156804.

15 P. S. Bagus, V. Staemmler and C. Wöll, *Phys. Rev. Lett.*, 2002, **89**, 096104.

16 J. C. P. Mignolet, *Discuss. Faraday Soc.*, 1950, **8**, 105–114.

17 S. Sadewasser and T. Glatzel, *Kelvin Probe Force Microscopy; Measuring and Compensating Electrostatic Forces*, Springer-Verlag, Berlin, Heidelberg, 2012.

18 G. H. Enevoldsen, T. Glatzel, M. C. Christensen, J. V. Lauritsen and F. Besenbacher, *Phys. Rev. Lett.*, 2008, **100**, 236104.

19 S. Kitamura and M. Iwatsuki, *Appl. Phys. Lett.*, 1998, **72**, 3154–3156.

20 S. Sadewasser, P. Jelínek, C.-K. Fang, O. Custance, Y. Yamada, Y. Sugimoto, M. Abe and S. Morita, *Phys. Rev. Lett.*, 2009, **103**, 266103.

21 A. Yurtsever, Y. Sugimoto, M. Fukumoto, M. Abe and S. Morita, *Appl. Phys. Lett.*, 2012, **101**, 083119.

22 L. Gross, B. Schuler, F. Mohn, N. Moll, N. Pavliček, W. Steurer, I. Scivetti, K. Kotsis, M. Persson and G. Meyer, *Phys. Rev. B: Condens. Matter*, 2014, **90**, 155455.

23 L. Nony, A. S. Foster, F. Bocquet and C. Loppacher, *Phys. Rev. Lett.*, 2009, **103**, 036802.

24 F. Bocquet, L. Nony and C. Loppacher, *Phys. Rev. B: Condens. Matter*, 2011, **83**, 035411.

25 A. Masago, M. Tsukada and M. Shimizu, *Phys. Rev. B: Condens. Matter*, 2010, **82**, 195433.

26 F. Krok, K. Sajewicz, J. Konior, M. Goryl, P. Piatkowski and M. Szymonski, *Phys. Rev. B: Condens. Matter*, 2008, **77**, 235427.

27 A. Sadeghi, A. Baratoff, S. A. Ghasemi, S. Goedecker, T. Glatzel, S. Kawai and E. Meyer, *Phys. Rev. B: Condens. Matter*, 2012, **86**, 075407.

28 J. L. Neff and P. Rahe, *Phys. Rev. B: Condens. Matter*, 2015, **91**, 085424.

29 L. Gross, F. Mohn, P. Liljeroth, J. Repp, F. J. Giessibl and G. Meyer, *Science*, 2009, **324**, 1428–1431.

30 T. Leoni, O. Guillermet, H. Walch, V. Langlais, A. Scheuermann, J. Bonvoisin and S. Gauthier, *Phys. Rev. Lett.*, 2011, **106**, 216103.

31 T. König, G. H. Simon, H.-P. Rust, G. Pacchioni, M. Heyde and H.-J. Freund, *J. Am. Chem. Soc.*, 2009, **131**, 17544–17545.

32 F. Mohn, L. Gross, N. Moll and G. Meyer, *Nat. Nanotechnol.*, 2012, **7**, 227–231.

33 F. Albrecht, J. Repp, M. Fleischmann, M. Scheer, M. Ondráček and P. Jelínek, *Phys. Rev. Lett.*, 2015, **115**, 076101.

34 J. Onoda, C. L. Pang, A. Yurtsever and Y. Sugimoto, *J. Phys. Chem. C*, 2014, **118**, 13674–13679.

35 C. Barth and C. R. Henry, *J. Phys. Chem. C*, 2009, **113**, 247–253.

36 C. Barth and C. R. Henry, *Appl. Phys. Lett.*, 2006, **89**, 252119.

37 C. Barth, A. S. Foster, C. R. Henry and A. L. Shluger, *Adv. Mater.*, 2011, **23**, 477–501.

38 E. Palacios-Lidón, C. R. Henry and C. Barth, *ACS Catal.*, 2014, **4**, 1838–1844.

39 A. Yurtsever, Y. Sugimoto, M. Abe and S. Morita, *Nanotechnology*, 2010, **21**, 165702.

40 G. H. Enevoldsen, A. S. Foster, M. C. Christensen, J. V. Lauritsen and F. Besenbacher, *Phys. Rev. B: Condens. Matter*, 2007, **76**, 205415.

41 G. H. Enevoldsen, H. P. Pinto, A. S. Foster, M. C. R. Jensen, A. Kühnle, M. Reichling, W. A. Hofer, J. V. Lauritsen and F. Besenbacher, *Phys. Rev. B: Condens. Matter*, 2008, **78**, 045416.

42 R. Bechstein, C. González, J. Schütte, P. Jelínek, R. Pérez and A. Kühnle, *Nanotechnology*, 2009, **20**, 505703.

43 A. Yurtsever, D. Fernández-Torre, C. González, P. Jelínek, P. Pou, Y. Sugimoto, M. Abe, R. Pérez and S. Morita, *Phys. Rev. B: Condens. Matter*, 2012, **85**, 125416.

44 A. Yurtsever, Y. Sugimoto, M. Abe, K. Matsunaga, I. Tanaka and S. Morita, *Phys. Rev. B: Condens. Matter*, 2011, **84**, 085413.

45 X. Mao, X. Lang, Z. Wang, Q. Hao, B. Wen, Z. Ren, D. Dai, C. Zhou, L.-M. Liu and X. Yang, *J. Phys. Chem. Lett.*, 2013, **4**, 3839–3844.

46 D. Fernández-Torre, A. Yurtsever, J. Onoda, M. Abe, S. Morita, Y. Sugimoto and R. Pérez, *Phys. Rev. B: Condens. Matter*, 2015, **91**, 075401.

47 V. Çelik, H. Ünal, E. Mete and Ş. Ellialtıoğlu, *Phys. Rev. B: Condens. Matter*, 2010, **82**, 205113.

48 H. Iddir, S. Öğüt, N. D. Browning and M. M. Disko, *Phys. Rev. B: Condens. Matter*, 2005, **72**, 081407.

49 E. Mete, O. Gülseren and Ş. Ellialtıoğlu, *Eur. Phys. J. B*, 2012, **85**, 204.

50 T.-Y. Chang, Y. Tanaka, R. Ishikawa, K. Toyoura, K. Matsunaga, Y. Ikuhara and N. Shibata, *Nano Lett.*, 2014, **14**, 134–138.

51 R. Souda, W. Hayami, T. Aizawa and Y. Ishizawa, *Surf. Sci.*, 1993, **285**, 265–274.

52 P. Hardman, R. Casanova, K. Prabhakaran, C. Muryn, P. Wincott and G. Thornton, *Surf. Sci.*, 1992, **269**, 677–681.

53 N. D. Lang and W. Kohn, *Phys. Rev. B: Solid State*, 1971, **3**, 1215.

54 C. Barth, T. Hynninen, M. Bieletzki, C. R. Henry, A. S. Foster, F. Esch and U. Heiz, *New J. Phys.*, 2010, **12**, 093024.

55 M. Tsukada, A. Masago and M. Shimizu, *J. Phys.: Condens. Matter*, 2012, **24**, 084002.

56 T. Arai and M. Tomitori, *Phys. Rev. Lett.*, 2004, **93**, 256101.

57 K. Okamoto, Y. Sugawara and S. Morita, *Appl. Surf. Sci.*, 2002, **188**, 381–385.

58 T. M. Salama, H. Hattori, H. Kita, K. Ebitani and T. Tanaka, *J. Chem. Soc., Faraday Trans.*, 1993, **89**, 2067–2073.

59 T. Huizinga, H. F. J. van'T Blik, J. C. Vis and R. Prins, *Surf. Sci.*, 1983, **135**, 580–596.

60 S. Lin, D. Sanders and M. Vannice, *J. Catal.*, 1994, **147**, 370–374.

61 K. D. Schierbaum, S. Fischer, M. C. Torquemada, J. L. de Segovia, E. Román and J. A. Martín-Gago, *Surf. Sci.*, 1996, **345**, 261–273.

62 A. Sasahara, C. L. Pang and H. Onishi, *J. Phys. Chem. B*, 2006, **110**, 13453–13457.

63 Y. Cai, Z. Bai, S. Chintalapati, Q. Zeng and Y. P. Feng, *J. Chem. Phys.*, 2013, **138**, 154711.

64 D. Çakir and O. Gülseren, *J. Phys. Chem. C*, 2012, **116**, 5735–5746.

65 S. C. Ammal and A. Heyden, *J. Chem. Phys.*, 2010, **133**, 164703.

66 A. Sasahara, C. L. Pang and H. Onishi, *J. Phys. Chem. B*, 2006, **110**, 17584–17588.

67 T. Kittel and E. Roduner, *J. Phys. Chem. C*, 2016, **120**, 8907–8916.

68 G. Kresse and J. Furthmüller, *Phys. Rev. B: Condens. Matter*, 1996, **54**, 11169–11186.

69 T. R. Albrecht, P. Grütter, D. Horne and D. Rugar, *J. Appl. Phys.*, 1991, **69**, 668–673.

70 H. Jing Chung, A. Yurtsever, Y. Sugimoto, M. Abe and S. Morita, *Appl. Phys. Lett.*, 2011, **99**, 123102.

71 J. P. Perdew, K. Burke and M. Ernzerhof, *Phys. Rev. Lett.*, 1996, **77**, 3865–3868.